nature materials

LETTERS

PUBLISHED ONLINE: 11 SEPTEMBER 2011 | DOI: 10.1038/NMAT3117

The role of nanopore shape in surface-induced crystallization

Ying Diao, Takuya Harada†, Allan S. Myerson, T. Alan Hatton and Bernhardt L. Trout*

Crystallization of a molecular liquid from solution often initiates at solid–liquid interfaces[1–3], and nucleation rates are generally believed to be enhanced by surface roughness[4,5]. Here we show that, on a rough surface, the shape of surface nanopores can also alter nucleation kinetics. Using lithographic methods, we patterned polymer films with nanopores of various shapes and found that spherical nanopores 15–120 nm in diameter hindered nucleation of aspirin crystals, whereas angular nanopores of the same size promoted it. We also show that favourable surface–solute interactions are required for angular nanopores to promote nucleation, and propose that pore shape affects nucleation kinetics through the alteration of the orientational order of the crystallizing molecule near the angles of the pores. Our findings have clear technological implications, for instance in the control of pharmaceutical polymorphism and in the design of 'seed' particles for the regulation of crystallization of fine chemicals.

It is well recognized that surfaces play a crucial role in liquid–solid phase transformations, and surface morphology has been shown to impact nucleation and crystallization significantly[6–8]. Current fundamental understanding is insufficient, however, to allow the rational design of surfaces for nucleation/crystallization control. Roughening of the surface in a crystallization system leads to accelerated nucleation, and in industrial practice surface scratching has long been used to promote nucleation[9]. However, without knowledge of the geometrical features of the surface cavities at a microscopic scale relevant to nucleation, the surface roughness alone, as a macroscopic parameter, may be insufficient, and even misleading, in describing the effect of surface morphology on nucleation. Recently, there has been an increase in the number of studies on crystal nucleation in sub-100 nm pores, which were demonstrated to affect nucleation kinetics[7,10,11], polymorphism[12] and crystal orientation[13]. These studies focused mainly on the effect of pore size in the context of nanoscopic confinement, but the role of pore shape has been neglected. The lack of systematic investigation on the effect of pore shape is due, in no small part, to the challenges in making macroscopic material with nanopores of tunable geometry, particularly with pores under 100 nm in size.

Here, we present the first experimental evidence that nanopore shape plays a key role in determining the kinetics of nucleation from solution. We are particularly interested in comparing the effects of angular pores to those of spherical pores of similar size. For this purpose, a fabrication technique is required to control both the surface pore geometry and the pore size down to length scales relevant to nucleation, and especially to enable surface patterning with pores from a few to hundreds of nanometres. Nanoscopic pores with high area density are preferred, providing a sufficient number of pores to ensure statistical significance of the observed effects on nucleation. Sub-10 nm pores are avoided because reported volume confinement effects on nucleation[11,14,15] may mask the effects of pore shape. In addition, the resolution requirement for the fabrication technique is set by the length scale of molecular events preceding nucleation, namely the molecular clustering and re-orientation that occur in domains of, probably, a few nanometres for small organic molecules. To meet these requirements, we developed 'Nanoparticle Imprint Lithography' (NpIL), drawing inspiration from Nanoimprint Lithography (NIL; ref. 16) and Nanosphere Lithography (NSL; ref. 17). NpIL can be used to fabricate nanopatterned polymer surfaces with nanopore arrays of various shapes, ranging from ten to hundreds of nanometres, using nanoparticle assemblies as templates.

The fabrication of polymer films with spherical nanopores by NpIL is illustrated in Fig. 1. First, spherical silica nanoparticles were self-assembled on a quartz slide driven by capillary forces during water evaporation[17], and then anchored to the substrate via calcination to form the imprint mould (Fig. 1a). Second, a mixture of monomer, crosslinker and initiator was sandwiched between the imprint mould and the substrate, and subsequently polymerized under ultraviolet irradiation. The imprint mould was then easily peeled off to reveal a polymer film conforming to the substrate, with the nanopattern inversely transferred from the imprint mould (Fig. 1b). Polymer films with spherical nanopores ranging from 15 nm to 300 nm were fabricated in this manner (Fig. 1c), templated by commercially available monodispersed colloidal silica of various sizes. This method combines many of the advantages of NSL and ultraviolet-assisted NIL, such as low cost, high throughput[18], and high resolution[16]. Moreover, in contrast to the commonly practiced NSL technique, where hydrofluoric acid is needed to dissolve the silica nanoparticles[17], our method removes the template nondestructively by a simple liftoff from the polymer film, allowing the mask to be recovered easily and reused.

Polymer films with hexagonal pores (Fig. 2a) were also prepared by NpIL following a similar procedure (see Methods section), templated with iron oxide magnetic nanocrystals with well-defined facets (Fig. 2b). For making square nanopores (Fig. 2c), square-shaped nanoposts (Fig. 2d) were fabricated by Achromatic Interference Lithography (AIL; ref. 19) as the imprint mould. The imprinted square pores are comparable to the spherical ones in width and depth (Fig. 2e), with sharply delineated pore angles (radius of curvature <3 nm, Supplementary Fig. S1). In addition, the nanopatterning procedures employed in this study preserved the molecular level surface roughness with respect to the nonporous polymer surface (Supplementary Table S1), which enables unambiguous differentiation of the effects of pore shape on crystal nucleation.

Department of Chemical Engineering, Massachusetts Institute of Technology, 77 Massachusetts Avenue, E19-502b, Cambridge, Massachusetts 02139, USA. †Present address: Nanotechnology Center, Yokohama R&D Laboratories, Furukawa Electric Co., Ltd., 2-4-3, Okano, Nishi-ku, Yokohama 220-0073, Japan. *e-mail: trout@MIT.EDU.

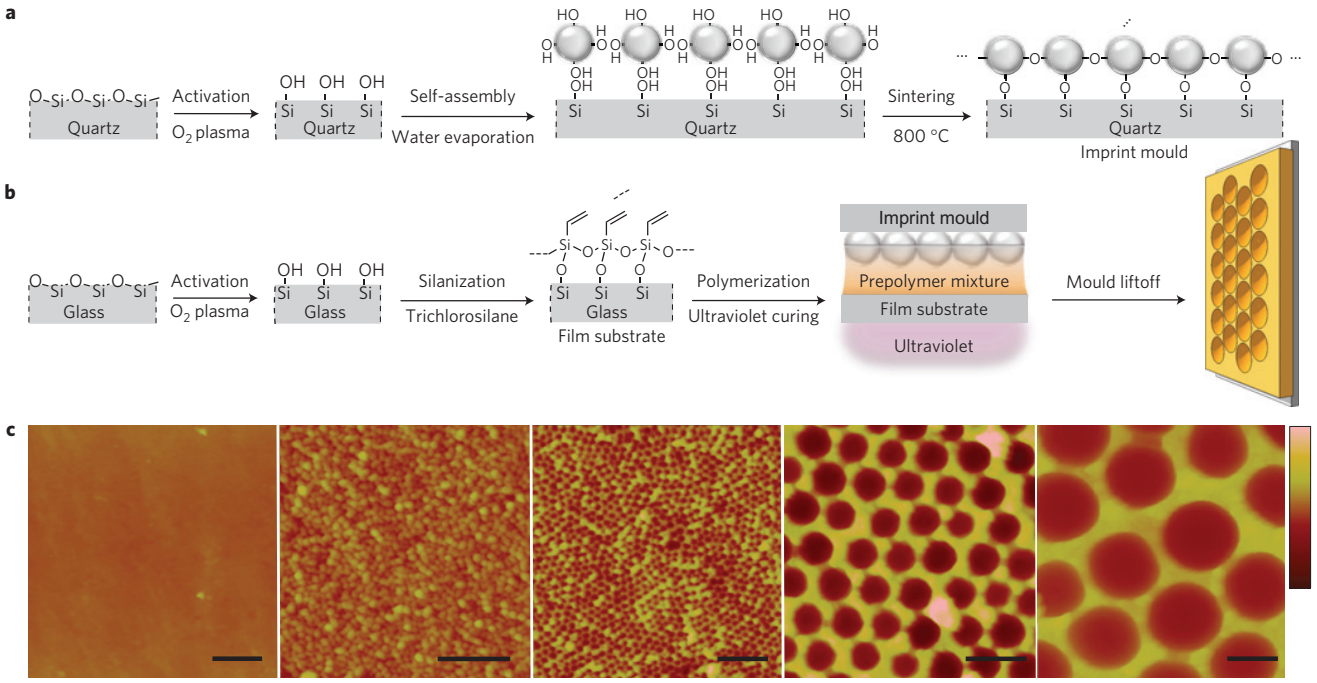

Figure 1 | Fabrication of polymer films with spherical nanopores by NpIL. a, Imprint mould preparation via colloidal silica self-assembly and its anchoring to the quartz substrate. **b**, Film substrate preparation and polymer film synthesis by ultraviolet polymerization. **c**, AFM height images of polyacrylic acid films crosslinked with divinylbenzene (AA-co-DVB), with and without spherical nanopores, templated with colloidal silica of various sizes. The average pore size is (from left to right) none, 15 nm, 40 nm, 120 nm, and 300 nm. The scale bar is 200 nm. The data scale in height is (from left to right) 50 nm, 50 nm, 50 nm, 100 nm and 400 nm.

The effect of nanopatterned polymer films on the kinetics of nucleation from solution was quantified by the nucleation induction time of aspirin (see Methods section), a representative compound for small organic molecules. The relative extent of reduction in the nucleation induction time serves as a measure of the effectiveness of polymer films in promoting nucleation. The polymer film was made from acrylic acid crosslinked with divinylbenzene (AA-co-DVB), with which aspirin could interact via hydrogen bonding. Polymer crosslinking was designed to avoid solvent uptake and to maintain the surface morphology when in contact with the solution. Owing to the stochastic nature of nucleation events, 20–50 samples were tested simultaneously to obtain the probability distribution for the nucleation induction time. The average induction time, τ, was determined from a statistical analysis of the induction time data, based on the knowledge that nucleation follows a Poisson distribution, $P(t) = \exp(-t/\tau)$ (ref. 7), where P is the probability that no nucleation event occurs within time t.

As shown in Fig. 3, increasing the surface roughness by modifying the nonporous film with spherical nanopores surprisingly inhibited nucleation, as evidenced by the longer nucleation induction times. The size of the spherical nanopores seemed to have little effect on the nucleation kinetics, within the range tested, but nucleation was promoted when angular pores of the same size were used, as shown in two cases. With hexagonal pores, the polymer film reduced aspirin nucleation induction times by more than an order of magnitude relative to those observed with spherical pores, and in the case of square pores, a three-fold reduction was observed. These results indicate that the angles that distinguish faceted from spherical pores acted as nucleation sites, which has been verified via atomic force microscopy (AFM) and X-ray diffraction (XRD), as will be discussed later. Our observations can be interpreted in terms of recent computational results. Cacciuto and co-workers[8] used Monte Carlo simulations to show that freezing of hard-sphere colloids is frustrated on curved surfaces, on which crystals cannot grow free of strain, and that the resulting defects increased the barrier to nucleation (see Supplementary Information Pages 8–9 for more discussion). Page and Sear found by Monte Carlo simulation of Lennard-Jones molecules that nucleation in wedges is many orders of magnitude faster than on a flat surface, and that there exists an optimum wedge angle at which nucleation is the fastest[9]. This optimum wedge angle corresponds to an intrinsic angle within the crystal, formed by two close-packed planes, at which the crystal can grow defect-free along both sides of the wedge.

'Angle-directed nucleation' is a possible mechanism in our case, where an angle characteristic of the topological feature on the substrate directs the crystal nucleation in a minimum-strain configuration, exhibited as a geometrical match between the substrate and the crystal. The aspirin crystal possesses intrinsic angles formed by close-packed, low-index facets close to the characteristic angles in the nanopores tested (Fig. 4c,d,f). In the square nanopore, the angle at the intersection of the pore wall and the pore floor (L_{wf}, its dihedral angle abbreviated as α) could induce the growth of either (011) and (100), or (002) and (100) facets of aspirin ((011) $\wedge$ (100) or (002) $\wedge$ (100), with dihedral angles abbreviated as $\theta_{011\wedge100}$ and $\theta_{002\wedge100}$, respectively; Fig. 4c,d), where (100), (011) and (002) are the three major facets of aspirin crystallized from bulk solution (Supplementary Fig. S4b). To estimate the extent of angular match, the cross-section of the square nanopore was examined by means of high-resolution scanning electron microscopy (HRSEM), and α was measured to be $96° \pm 7°$ in one corner of the cross-section and $101° \pm 5°$ in the other. This asymmetry was consistent through the cross-section for all pores observed, and may arise from the asymmetric stress applied to the polymer film during the template liftoff. Both $\theta_{011\wedge100}$ and $\theta_{002\wedge100}$ fall in the vicinity of the smaller α, $96 \pm 7°$, with $\theta_{002\wedge100}$ being the closer match ($\theta_{002\wedge100} = 95.84°$, $\theta_{011\wedge100} = 92.94°$). Specifically, about 30% of pores contained an angle α within 1° of $\theta_{002\wedge100}$, and around 8% within 1° of $\theta_{011\wedge100}$.

If angle-matching were the only factor dictating nanopore-induced nucleation, (002) $\wedge$ (100) would be nucleated preferentially

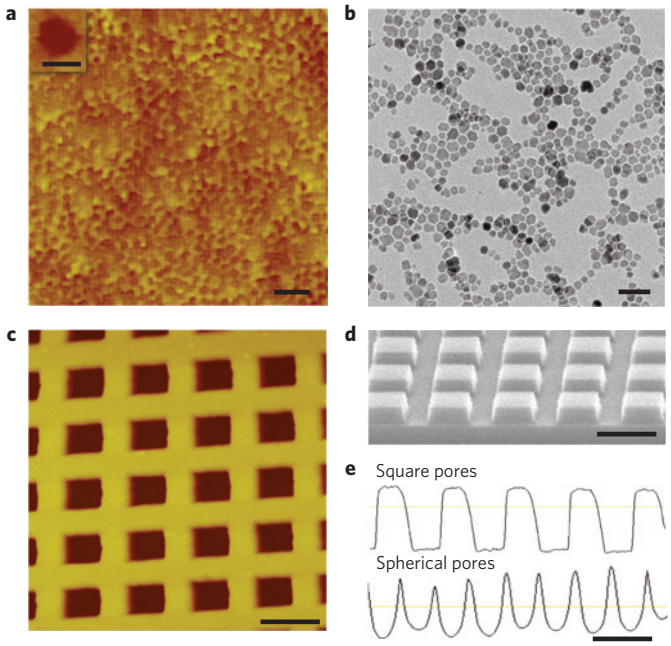

Figure 2 | Angular nanopores on AA-co-DVB polymer films and their templates. a, AFM height image of hexagonal nanopores on the polymer surface templated with iron oxide magnetic nanocrystals by means of NpIL. The scale bar is 50 nm. (Inset) Higher resolution image of a hexagonal nanopore. The scale bar is 10 nm. **b**, Transmission electron microscopy image of iron oxide magnetic nanocrystals as synthesized. The scale bar is 50 nm. **c**, AFM height image of square nanopores on the polymer surface templated with Si square posts. The scale bar is 200 nm. **d**, High-resolution SEM image of Si square posts on a Si wafer fabricated by AIL for templating square pores. The scale bar is 200 nm. **e**, Depth profiles of square and spherical nanopores of similar sizes. The scale bar is 200 nm. The square pores are 125 nm in width and 48 nm in depth, and the spherical pores are 120 nm in width and 45 nm in depth, on average.

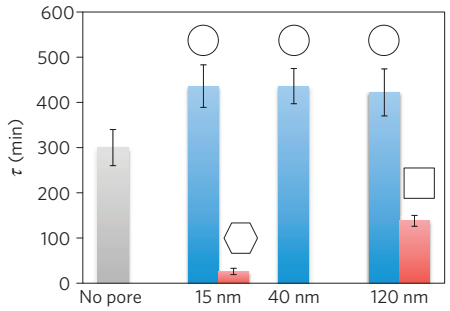

Figure 3 | Effect of the nanopore shape in AA-co-DVB polymer films on the nucleation kinetics of aspirin: spherical pores versus hexagonal pores and square pores of the same size. Nanopatterned surfaces are compared against flat and smooth surfaces without pores, labelled as 'no pore'. τ is the average nucleation induction time. The standard errors of τ were calculated from the regression on the induction time probability distribution following the Poisson distribution.

from L_{wf} within the pore. The AFM images of aspirin crystals grown from the pores suggest it was the (011) ∧ (100) facets that emanated from L_{wf}, whereas the (002) facet was not in contact with the pore surface (Fig. 4a,b; Supplementary Fig. S2; see Supplementary Information Page 5 for assignment of crystal facets). Layered growth of aspirin parallel to the pore floor is evident in both the crystal grown out from the pore (Fig. 4a) and the crystals contained in the pore (Fig. 4b), which originates from the aspirin dimerization through the carboxyl group within the (100) layer, and a much weaker van der Waals interaction between the layers. Figure 4b shows that these (100) crystal layers seem to extend from the pore wall with which the (011) face is in contact. Moreover, the layer extension direction, as denoted by white arrows, is consistent in all pores containing crystals, indicating nucleation occurs predominantly from one side of the pore. In addition, only a fraction of the pores induced nucleation. These observations provide evidence that the (011) ∧ (100) and not (002) ∧ (100) facets were nucleated from L_{wf}, but only from those with the appropriate angle α. These growth patterns can be attributed to the favourable interactions between (011) ∧ (100) and the polymer surface, as inferred from the characteristic functionalities exhibited on their respective surfaces (Fig. 4c–e). (011) and (100) planes, rich in carboxyl and carbonyl groups, can form hydrogen bonds with the carboxyl groups on the AA-co-DVB polymer surface, whereas the nonpolar (002) plane is likely to interact with the polymer much more weakly. This result suggests that solute–polymer interactions, and not just the geometrical match, play an important role in determining nucleation behaviour in angular pores. Directed by both favourable interactions and angular match, the single crystals in square nanopores exhibited a high degree of alignment (Supplementary Figs S4, S5), providing further evidence for nucleation at pore angles.

Following the principle of angle-directed nucleation assisted by favourable interactions, we propose that the corners within hexagonal pores acted as nucleation sites to induce the growth of (011) ∧ (01$\bar{1}$) ∧ (100), where (100) was in contact with the pore floor, and (011) ∧ (01$\bar{1}$) were in contact with the pore walls (Fig. 4f). This is plausible because the angle mismatch is very small in this configuration, and all three faces of aspirin could interact with the polymer surface through hydrogen bonding. If nucleation ensued from the corner, the growth thereafter would have resulted in an aspirin crystallite that fitted comfortably inside the pore and took on the shape of a hexagon, given that the other intrinsic angles of the crystal also matched fairly well with the pore geometry (Fig. 4h). Indeed, crystallites with comparable shape and size to those of the pore were observed via AFM on the surface of aspirin crystals detached from the polymer film (Fig. 4g,i). In addition, XRD results verified that the (100) face was in contact with the pore floor (Supplementary Fig. S3). Moreover, in-plane alignment of hexagonal crystallites was also evident in local domains (Supplementary Fig. S6). These observations support our hypothesis of corner-induced nucleation from hexagonal pores.

On the basis of the experimental and computational evidence, we propose a molecular mechanism to interpret the pore shape effect on nucleation. Crystal nucleation from solution is preceded by molecular cluster formation through density fluctuations and molecular re-orientation through structure fluctuations; both are necessary for nucleation[20–23]. The rate of nucleation can be modified in two ways by the presence of an amorphous, nanoporous surface in a metastable solution. First, favourable surface–solute interactions enrich solute concentrations near the surface, and molecular recognition events between the surface and the solute induce partial orientational order in the enriched solute layers; both effects could facilitate nucleus formation[7,24,25]. Second, angles in the pore further enhance the orientational order of the solute in domains close to the surface by means of geometrical confinement, which facilitates the solute molecular realignment during nucleus formation. When the molecular orientation imposed by the angle geometry resembles that in the crystal, the rate of nucleation is increased to the greatest extent, the macroscopic expression of which is angle-directed nucleation.

As implied by our hypothesis, favourable surface–solute interaction is a prerequisite for angular nanopores to promote nucleation. To verify this point, we changed the chemical makeup of the polymer film from AA-co-DVB to AM-co-DVB (Fig. 5).

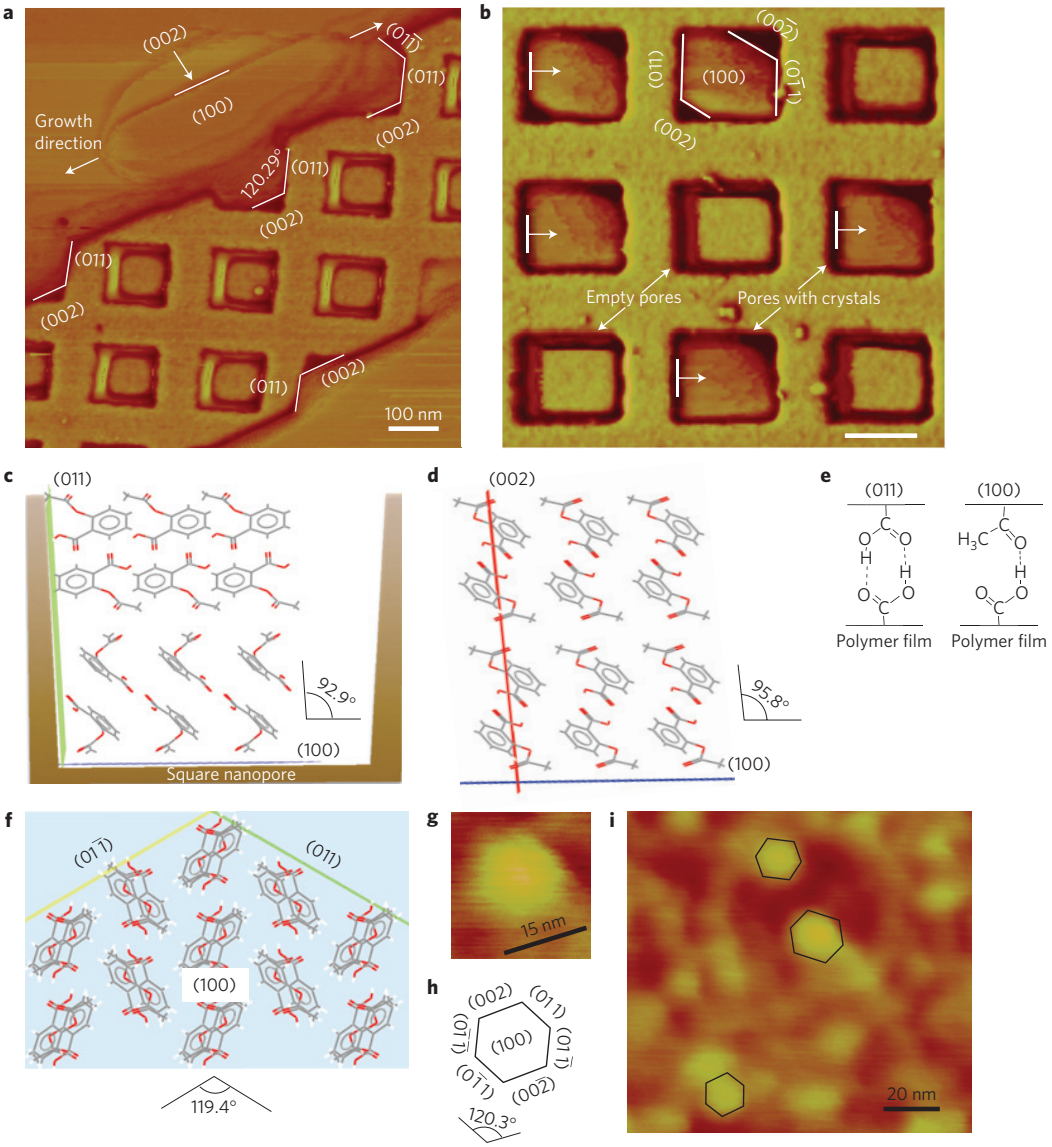

Figure 4 | Angle-directed nucleation of aspirin crystals induced by angular nanopores. a, AFM phase image of aspirin crystals grown out from the square pores. **b**, AFM phase image showing (100) layers of aspirin crystals nucleated at ledges in the square pores, indicated with white lines for all pores containing crystals. The scale bar is 100 nm. **c**,**d**, Possible configurations of aspirin crystal facets in the square pore, with the cross-section depicted. **e**, Proposed aspirin–polymer interactions at the crystal-polymer interface. Between (100) and the polymer, the methyl hydrogen of (100) could interact with the carbonyl oxygen of the polymer via a secondary hydrogen bond, which is not shown in the depiction. **f**, Proposed configuration of aspirin crystal facets at the corner of a hexagonal pore. **g**,**h**, AFM phase image of an aspirin crystallite grown from the 15 nm hexagonal pores and its possible orientation. **i**, AFM height image of the surface of an aspirin crystal grown on and detached from the AA-co-DVB polymer film with hexagonal pores. The contours of the crystallites are traced at a small distance from the crystal edges so as not to obscure them.

This chemistry was selected out of the polymer films tested because, in the absence of pores, it exhibited no effect on aspirin nucleation from butyl acetate, indicating that surface–solute interactions are not sufficiently strong to affect nucleation under these conditions (Supplementary Fig. S7). As expected, patterning of the AM-co-DVB surface with the same angular nanopores did not lead to enhanced nucleation kinetics relative to nucleation on nonporous films (Fig. 5). With our new insight, nanostructured materials can be designed to cater for a variety of applications, from controlling pharmaceutical polymorphism to inhibiting ice nucleation on airplanes.

Methods

Fabrication of polymer films with spherical nanopores. Quartz slides (75 mm × 25 mm) were treated with O_2 plasma to enrich the surface in hydroxyl groups. Two hundred microlitres of 5w% colloidal silica (commercially available) were spread on the quartz slide and allowed to self-assemble during slow water evaporation over 12 h. The self-assembled SiO_2 and the quartz slide were then sintered at 800 °C for 5 min to coalesce the particles with the quartz slide and form the imprint mould. The film substrate (25 mm × 5 mm) was prepared by treating a glass slide with O_2 plasma, followed by silanization with trichlorosilane in a vacuum oven at 40 °C. Silanization is necessary to 'glue' the polymer film to the substrate via covalent bonds and thereby avoid film cracking and peeling from the substrates. One microlitre prepolymer mixture of monomer acrylic acid (AA), crosslinker divinylbenzene (DVB), and initiator IRGACURE 2022 were sandwiched between the imprint mould and the film substrate. The molar ratio of monomer to DVB was 2:1. The concentration of IRGACURE 2022 was 4 v% with respect to DVB. The prepolymer mixture was then polymerized under ultraviolet irradiation for 15 min, at 72 mW cm^{-2}. After irradiation, the imprint mould was peeled off and the polymer films were annealed at 70 °C in a vacuum oven for 3 h to remove unreacted species. Whenever possible, parts were pre-cleaned and assembled in a Bio-Safety cabinet to reduce contamination by impurities, which can interfere with polymer film induced nucleation.

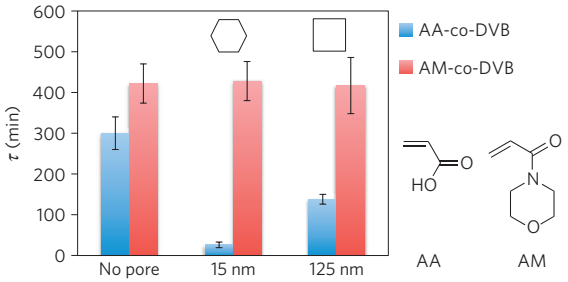

Figure 5 | Effect of polymer surface chemistry on the kinetics of angular nanopore-induced nucleation of aspirin: AA-co-DVB versus AM-co-DVB. τ is the average nucleation induction time. AM denotes 4-acryloylmorpholine. AA denotes acrylic acid. AM-co-DVB denotes poly 4-acryloylmorpholine crosslinked with divinylbenzene.

Fabrication of polymer films with angular nanopores. Polymer films with hexagonal nanopores were synthesized following a procedure similar to that described above, templated with iron oxide magnetic nanoparticles (MNP). The nanoparticle synthesis scheme is included on Page 1 of the Supplementary Information. The presence of sufficient surfactants (oleic acid) during synthesis was important for obtaining sharply defined facets of MNP crystals. As in the case of producing spherical nanopores, colloidal self-assembly was used to prepare the imprint mould, which was made by spreading 20 µl MNP-decane solution (~9 w%) on a plasma cleaned quartz slide (75 mm × 25 mm) and allowing the decane to evaporate over a period of 6 h. The excessive surfactants present in the nanocrystal dispersion also participated in the assembly process, leaving space for polymers to form between the nanocrystals. After polymerization, the imprint mould was peeled off from the polymer film, the nanocrystals on the film were subsequently dissolved with dilute hydrocholoric acid (~1N), and the film was rinsed with deionized water, then with acetone, and vacuum dried. The imprint mould for making square pores was fabricated by (AIL; ref. 19) at the MIT Research Laboratory of Electronics. The mould took the form of 125 nm Si square pillar arrays with a 200 nm pitch covering a 3-inch Si wafer. The top edges of the pillars were sharply defined, with radii of curvature less than 5 nm. Large area patterning is necessary to make sufficient copies of polymer films to obtain the induction time probability distribution. The polymer-film synthesis and post-processing procedures were the same as those used in the preparation of spherical nanopores. The effects of polymer films with pores on nucleation kinetics were compared against those in the absence of pores, which were synthesized following the same procedure, with the quartz surface as the template.

Nucleation induction time measurement. Once synthesized, the polymer film with its substrate was inserted vertically into a 1 ml glass shell vial containing 200 µl 47 mg ml^{-1} aspirin solution in butyl acetate. For each polymer sample, 20–50 vials were assembled and immersed in a circulator stabilized at 50 ± 0.1 °C to dissolve any pre-existing crystals, and then the solution was quench cooled to 5 ± 0.1 °C by immersing into a second circulator. The supersaturation at the start of each experiment was 2.2, defined as the ratio of starting concentration to the equilibrium concentration at the crystallization temperature. The number of vials in which crystallization occurred was recorded as a function of time. All the operations involving exposing polymer films, aspirin solutions and shell vials to the atmosphere were conducted inside a Bio-Safety cabinet to reduce impurity contamination to the lowest possible level. Efforts were made to clean all components before use, and aspirin solutions were filtered with an Acrodisc 0.2 µm PTFE syringe filter.

Characterization. AFM and XRD were employed to study the aspirin crystal orientation inside the angular nanopores on the polymer films following the nucleation induction time study. AFM images were obtained with a Dimension 3100 XY closed loop scanner (Nanoscope IV, VEECO) equipped with NanoMan software. Height and phase images were obtained in tapping mode in ambient air with silicon tips (VEECO). The crystal orientation was verified with XRD to identify the specific crystallographic planes parallel to the polymer film. The X-ray diffraction patterns were recorded with a PANalytical X'Pert PRO Theta/Theta Powder X-Ray Diffraction System with a Cu tube and X'Celerator high-speed detector. No fewer than five polymer films were examined with XRD on each type of polymer sample.

Received 7 April 2011; accepted 10 August 2011; published online 11 September 2011

References

1. Debenedetti, P. G. *Metastable Liquids: Concepts and Principles* (Princeton Univ. Press, 1996).
2. Mullin, J. W. *Crystallization* 4th edn (Butterworth-Heinemann, 2001).
3. Turnbull, D. Kinetics of heterogeneous nucleation. *J. Chem. Phys.* **18,** 198–203 (1950).
4. Curcio, E., Curcio, V., Di Profio, G., Fontananova, E. & Drioli, E. Energetics of protein nucleation on rough polymeric surfaces. *J. Phys. Chem. B* **114,** 13650–13655 (2010).
5. Briseno, A. L. *et al.* Patterning organic single-crystal transistor arrays. *Nature* **444,** 913–917 (2006).
6. Ward, M. D. Bulk crystals to surfaces: Combining X-ray diffraction and atomic force microscopy to probe the structure and formation of crystal interfaces. *Chem. Rev.* **101,** 1697–1725 (2001).
7. Diao, Y., Myerson, A. S., Hatton, T. A. & Trout, B. L. Surface design for controlled crystallization: The role of surface chemistry and nanoscale pores in heterogeneous nucleation. *Langmuir* **27,** 5324–5334 (2011).
8. Cacciuto, A., Auer, S. & Frenkel, D. Onset of heterogeneous crystal nucleation in colloidal suspensions. *Nature* **428,** 404–406 (2004).
9. Page, A. J. & Sear, R. P. Crystallization controlled by the geometry of a surface. *J. Am. Chem. Soc.* **131,** 17550–17551 (2009).
10. Chayen, N. E., Saridakis, E. & Sear, R. P. Experiment and theory for heterogeneous nucleation of protein crystals in a porous medium. *Proc. Natl Acad. Sci. USA* **103,** 597–601 (2006).
11. Diao, Y. *et al.* Controlled nucleation from solution using polymer microgels. *J. Am. Chem. Soc.* **133,** 3756–3759 (2011).
12. Ha, J. M., Wolf, J. H., Hillmyer, M. A. & Ward, M. D. Polymorph selectivity under nanoscopic confinement. *J. Am. Chem. Soc.* **126,** 3382–3383 (2004).
13. Hamilton, B. D., Weissbuch, I., Lahav, M., Hillmyer, M. A. & Ward, M. D. Manipulating crystal orientation in nanoscale cylindrical pores by stereochemical inhibition. *J. Am. Chem. Soc.* **131,** 2588–2596 (2009).
14. Jackson, C. L. & McKenna, G. B. Vitrification and crystallization of organic liquids confined to nanoscale pores. *Chem. Mater.* **8,** 2128–2137 (1996).
15. Maheshwari, P. *et al.* Effect of interfacial hydrogen bonding on the freezing/melting behavior of nanoconfined liquids. *J. Phys. Chem. C* **114,** 4966–4972 (2010).
16. Stewart, M. D. & Willson, C. G. Imprint materials for nanoscale devices. *MRS Bull.* **30,** 947–951 (2005).
17. Xia, Y. N., Gates, B., Yin, Y. D. & Lu, Y. Monodispersed colloidal spheres: Old materials with new applications. *Adv. Mater.* **12,** 693–713 (2000).
18. Trujillo, N. J., Baxamusa, S. H. & Gleason, K. K. Grafted functional polymer nanostructures patterned bottom-up by colloidal lithography and initiated chemical vapor deposition (iCVD). *Chem. Mater.* **21,** 742–750 (2009).
19. Savas, T. A., Schattenburg, M. L., Carter, J. M. & Smith, H. I. Large-area achromatic interferometric lithography for 100 nm period gratings and grids. *J. Vacuum Sci. Technol. B* **14,** 4167–4170 (1996).
20. tenWolde, P. R. & Frenkel, D. Enhancement of protein crystal nucleation by critical density fluctuations. *Science* **277,** 1975–1978 (1997).
21. Erdemir, D., Lee, A. Y. & Myerson, A. S. Nucleation of crystals from solution: Classical and two-step models. *Acc. Chem. Res.* **42,** 621–629 (2009).
22. Santiso, E. E. & Trout, B. L. A general set of order parameters for molecular crystals. *J. Chem. Phys.* **134,** 064109 (2011).
23. Vekilov, P. G. Dense liquid precursor for the nucleation of ordered solid phases from solution. *Cryst. Growth Des.* **4,** 671–685 (2004).
24. van Meel, J. A., Sear, R. P. & Frenkel, D. Design principles for broad-spectrum protein-crystal nucleants with nanoscale pits. *Phys. Rev. Lett.* **105,** 205501 (2010).
25. Dey, A. *et al.* The role of prenucleation clusters in surface-induced calcium phosphate crystallization. *Nature Mater.* **9,** 1010–1014 (2010).

Acknowledgements

We acknowledge the Novartis-MIT Center for Continuous Manufacturing for funding. We are grateful to T. Savas at MIT Research Laboratory of Electronics for fabricating the imprint mould with Si square nanopillars and to K. Gleason for use of her equipment for plasma treatment and glass silanization.

Author contributions

Y.D. designed, carried out the experiments and wrote the manuscript. B.L.T., T.A.H. and A.S.M. supervised the work, guided and revised the manuscript. T.H. synthesized and characterized the Fe_3O_4 magnetic nanoparticles and co-wrote the Supplementary Information.

Additional information

The authors declare no competing financial interests. Supplementary information accompanies this paper on www.nature.com/naturematerials. Reprints and permissions information is available online at http://www.nature.com/reprints. Correspondence and requests for materials should be addressed to B.L.T.